中正嶺學報 第三十三卷 第二期 民國 94.5.
JOURNAL OF C.C.I.T., VOL.33, NO.2, MAY, 2005

SHAPE OPTIMIZATION ON DOUBLE-CHAMBER MUFFLER WITH SIDE INLET/OUTLET UNDER SPACE CONSTRAINT

Ying-Chun Chang, Long-Jyi Yeh, Min-Chie Chiu, and Gaung-Jer Lai

Department of Mechanical Engineering, Tatung University

ABSTRACT

The accessory facility of noise abatement is often confined for the necessity of equipment's maintenance and operation; therefore, how to ultimate the acoustic performance of mufflers within a limited space becomes an essential issue. This paper proposes an optimal design of a muffler with two expansion chambers (hybridized with inlet and outlet tubes) under maximal sound transmission loss (STL) considerations. A graphic analysis system together with the two powerful gradient techniques is also described in detail. A set of initial design data is primarily derived via computer graphic analysis on sensitivity. The shape optimization of a muffler is then carried out using the successive algorithm of iteration techniques. The results are not only summarized but also compared with each other. In order to determine the accuracy of this study, the results are confirmed using the Kuhn-Tucker Condition. A numerical case illustrating the elimination of pure tone noise is also introduced. Results reveal that the sound transmission loss (STL) is maximized at the desired frequency. This study reinforces the quick and effective approach of an optimal design for double-chamber mufflers under space.

Keywords*:* four-pole matrix, shape optimization, double-chamber muffler with side inlet/outlet

限制空間下的雙腔邊進排氣式消音器的外型最佳化設計

張英俊　葉隆吉　邱銘杰　賴光哲

大同大學機械工程學系

摘　　要

為配合維修與操作，附屬的防音設備空間常受到限制，因而，如何在空間限制下將消音器的減音性能極大化，即為一極為重要的訴求。本文討論邊進出氣式雙腔消音器的外型最佳化設計，文中同時說明電腦圖形判別與二種功能強大的梯度數值分析技巧。一組初始設計參數可藉由電腦的靈敏度圖形判別系統中獲得，後續的數值技巧則將依據上述的初始設計參數進行搜尋，上述二法之解亦被匯整並互做比較。此外，為了驗證數值最佳化後的結果精確度，將引用 Kuhn-Tucker Condition 法則來驗證，本文中引用一個單頻音的控制為最佳化的範例探討，結果顯示，經過最佳化處理後，聲音穿透損失值(STL)確實在設計頻率處被極大化，本研究主要強調一種快速且有效的最佳化設計方法，可用在限制尺寸下的邊進出氣式雙腔消音器的設計上。

關鍵字：四埠傳輸矩陣，外型最佳化，雙腔邊進排氣式消音器

文稿收件日期 92.11.3; 文稿修正後接受日期 93.10.27.
Manuscript received Nov. 3, 2003; revised Oct. 27, 2004.

I. INTRODUCTION

A muffler is considered a kind of passive noise elimination device. It is usually used in venting equipment such as a diesel engine [1]. Nevertheless, mufflers are often constrained by the availability of space. Therefore, there has been increasing interest in designing mufflers in order to maximize the STL using shape optimization under space constraints.

Many researches on mufflers were well developed [2, 3, 4]. However, there has been difficulty in obtaining discussions of the shape optimization on mufflers. In 1986, Bernhard [5] introduced the shape optimization of simple expansion mufflers using non-constrained design space. Bernhard also developed sensitivity matrices in order to judge the global maximum. The constrained problem involves operation and maintenance concerns in practical engineering work. In addition, there has been difficulty in calculating design sensitivity matrices for mufflers with complicated mechanisms. Previous research [6] reveals that the graphic analysis method can be used in obtaining the optimal shape of single expansion mufflers. In order to improve the STL on mufflers and obtain accurate optimal design solutions, a new double-chamber muffler with side inlet and outlet is used. Mathematical gradient methods are also adopted in this study. In addition, the four-pole matrix [2, 3, 4] is used in evaluating the STL of mufflers (based on the plane wave theory).

This paper also proposes a method to obtain an optimal design data for mufflers by using a computer graphic system and gradient methods [7, 8]. This includes the exterior penalty function method (EPFM) and the interior penalty function method (IPFM). A numerical case of a muffler with double chambers (hybridized with an inlet/outlet tube) is also illustrated in order to demonstrate the advantages of this study.

II. THEORETICAL BACKGROUND

A 3-D cross-section of the double chamber muffler (hybridized with side inlet/outlet tube) is shown in Fig.1.

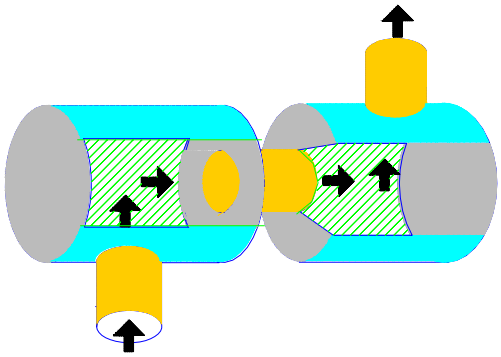

Fig.1. 3-D cross-section for a double-chamber muffler hybridized with side inlet/outlet tube.

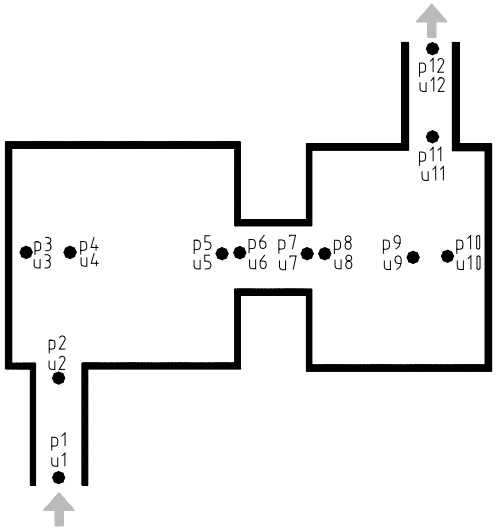

Fig.2. Flow condition for a double-chamber muffler hybridized with side inlet/outlet and tube.

Additionally, the flow condition and location of the muffler is specified in Fig.2. Besides,

the corresponding dimensions of the outline with respect to each part of the muffler are symbolized and depicted in Fig. 3.

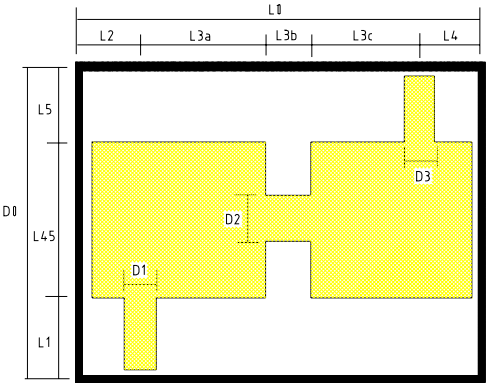

Fig.3. Space constraints for a double-chamber muffler hybridized with side inlet/outlet tube.

In Fig. 2, it is observed that the whole flow condition of the muffler can be presented by twelve nodes (pt1~pt12). The transfer matrix of the muffler system is deduced and described as follows:

2.1 Straight duct [4]

As derived by Prasad [2], an alternative form of the four-pole matrix between points 1 and 2 (with mean flow) is expressed in Eq. (1)

$$\begin{pmatrix} p_1 \\ \rho_o c_o u_1 \end{pmatrix} = e^{-jM_1 kL_1/(1-M_1^2)} \begin{bmatrix} \cos\left(\frac{kL_1}{1-M_1^2}\right) & j\sin\left(\frac{kL_1}{1-M_1^2}\right) \\ j\sin\left(\frac{kL_1}{1-M_1^2}\right) & \cos\left(\frac{kL_1}{1-M_1^2}\right) \end{bmatrix} \begin{pmatrix} p_2 \\ \rho_o c_o u_2 \end{pmatrix} \quad (1)$$

As derived in Eq. (1), the four-pole matrix between points 4 and 5 (with mean flow) is expressed in Eq. (2)

$$\begin{pmatrix} p_4 \\ \rho_o c_o u_4 \end{pmatrix} = e^{-jM_4 kL_{3a}/(1-M_4^2)} \begin{bmatrix} \cos\left(\frac{kL_{3a}}{1-M_4^2}\right) & j\sin\left(\frac{kL_{3a}}{1-M_4^2}\right) \\ j\sin\left(\frac{kL_{3a}}{1-M_4^2}\right) & \cos\left(\frac{kL_{3a}}{1-M_4^2}\right) \end{bmatrix} \begin{pmatrix} p_5 \\ \rho_o c_o u_5 \end{pmatrix} \quad (2)$$

Similarly, the four-pole matrix between points 6 and 7 (with mean flow) is expressed in Eq. (3)

$$\begin{pmatrix} p_6 \\ \rho_o c_o u_6 \end{pmatrix} = e^{-jM_6 kL_{3b}/(1-M_6^2)} \begin{bmatrix} \cos\left(\frac{kL_{3b}}{1-M_6^2}\right) & j\sin\left(\frac{kL_{3b}}{1-M_6^2}\right) \\ j\sin\left(\frac{kL_{3b}}{1-M_6^2}\right) & \cos\left(\frac{kL_{3b}}{1-M_6^2}\right) \end{bmatrix} \begin{pmatrix} p_7 \\ \rho_o c_o u_7 \end{pmatrix} \quad (3)$$

The four-pole matrix between points 8 and 9 is expressed in Eq. (4)

$$\begin{pmatrix} p_8 \\ \rho_o c_o u_8 \end{pmatrix} = e^{-jM_8 kL_{3c}/(1-M_8^2)} \begin{bmatrix} \cos\left(\frac{kL_{3c}}{1-M_8^2}\right) & j\sin\left(\frac{kL_{3c}}{1-M_8^2}\right) \\ j\sin\left(\frac{kL_{3c}}{1-M_8^2}\right) & \cos\left(\frac{kL_{3c}}{1-M_8^2}\right) \end{bmatrix} \begin{pmatrix} p_9 \\ \rho_o c_o u_9 \end{pmatrix} \quad (4)$$

And the four-pole matrix between points 11 and 12 is expressed in Eq. (5)

$$\begin{pmatrix} p_{11} \\ \rho_o c_o u_{11} \end{pmatrix} = e^{-jM_{11} kL_5/(1-M_{11}^2)} \begin{bmatrix} \cos\left(\frac{kL_5}{1-M_{11}^2}\right) & j\sin\left(\frac{kL_5}{1-M_{11}^2}\right) \\ j\sin\left(\frac{kL_5}{1-M_{11}^2}\right) & \cos\left(\frac{kL_5}{1-M_{11}^2}\right) \end{bmatrix} \begin{pmatrix} p_{12} \\ \rho_o c_o u_{12} \end{pmatrix} \quad (5)$$

2.2 Side inlet/ side outlet duct [3]

As derived by Munjal [3], the four-pole matrix between points 2 and 4 (with mean flow) is expressed in Eq. (6)

$$\begin{pmatrix} p_2 \\ v_2 \end{pmatrix} = \begin{bmatrix} 1-\frac{M_2 Y_2}{Z_3} & (1+k_e)M_4 Y_4 - M_2 Y_2 + Y_2(j0.85kD_1/2) \\ \frac{1}{Z_3} & 1 \end{bmatrix} \begin{pmatrix} p_4 \\ v_4 \end{pmatrix} \quad (6a)$$

where $Z_3 = -j\frac{c_o}{S_3}\cot(kL_2)$; $Y_3 = Y_4 = \frac{c_o}{S_4}$;

$$Y_2 = \frac{c_o}{S_2} \ ; \ k_e = \left[\left(\frac{S_4}{S_2}\right) - 1\right]^2 \quad (6b)$$

Instead of v (the acoustic mass velocity), u (acoustic particle velocity) is adopted in Eq. (6a). An equivalent form is derived in Eq. (7)

$$\begin{pmatrix} p_2 \\ \rho_o c_o u_2 \end{pmatrix} = \begin{bmatrix} Ts2_{1,1} & Ts2_{1,2} \\ Ts2_{2,1} & Ts2_{2,2} \end{bmatrix} \begin{pmatrix} p_4 \\ \rho_o c_o u_4 \end{pmatrix} \quad (7a)$$

Where $Ts2_{1,1} = 1 - j\frac{M_2 S_3}{S_2}\tan(kL_2)$;

$$Ts2_{1,2} = \left(M_4\left[1+\left(\frac{S_4}{S_2}-1\right)^2\right] - M_2\frac{S_4}{S_2}\right) \ ; \\ + j\left(\frac{0.85kD_1}{2}\right)\frac{S_4}{S_2}$$

$$Ts2_{2,1} = j\frac{S_3}{S_2}\tan(kL_2) \, ; Ts2_{2,2} = \frac{S_4}{S_2} \quad (7b)$$

As described in Eq. (7), the four-pole matrix between points 9 and 11 (with mean flow) is expressed in Eq. (8)

$$\begin{pmatrix} p_9 \\ v_9 \end{pmatrix} = \begin{bmatrix} 1-\frac{M_9 Y_9}{Z_{10}} & (1+k_c)M_{11}Y_{11} - M_9 Y_9 + Y_{11}(j\frac{0.85kD_3}{2}) \\ \frac{1}{Z_{10}} & 1+\frac{M_{11}Y_{11}-M_9 Y_9}{Z_{10}} \end{bmatrix} \begin{pmatrix} p_{11} \\ v_{11} \end{pmatrix} \quad (8a)$$

where $Z_{10} = -j\frac{c_o}{S_9}\cot(kL_4)$; $Y_9 = Y_{10} = \frac{c_o}{S_9}$;

$$Y_{11} = \frac{c_o}{S_{11}} \ ; \ k_c = \left(1-\frac{S_{11}}{S_9}\right)/2 \quad (8b)$$

Instead of v (the acoustic mass velocity), u (acoustic particle velocity) is adopted. An equivalent form is derived in Eq. (9)

$$\begin{pmatrix} p_9 \\ \rho_o c_o u_9 \end{pmatrix} = \begin{bmatrix} Ts4_{1,1} & Ts4_{1,2} \\ Ts4_{2,1} & Ts4_{2,2} \end{bmatrix} \begin{pmatrix} p_{11} \\ \rho_o c_o u_{11} \end{pmatrix} \quad (9a)$$

Where $Ts4_{1,1} = 1 - j\frac{M_9 S_{10}}{S_5}\tan(kL_2)$;

$$Ts4_{1,2} = \left(M_{11}\left[1+\frac{1-S_{11}/S_9}{2}\right] - M_9\frac{S_{11}}{S_9}\right) \ ; \\ + j\left(\frac{0.85kD_2}{2}\right)$$

$$Ts4_{2,1} = j\frac{S_{10}}{S_9}\tan(kL_4) \ ;$$

$$Ts4_{2,2} = \frac{S_{11}}{S_9} + j\left[M_{11}\frac{S_{10}}{S_9} - M_9\frac{S_{10}S_{11}}{S_9^2}\right]\tan(kL_4) \quad (9b)$$

2.3 Expansion/contraction duct [4]

As derived by Munjal [4], the four-pole matrix between points 5 and 6 (with mean flow) is expressed in Eq. (10)

$$\begin{pmatrix} p_5 \\ \rho_o c_o u_5 \end{pmatrix} = \begin{bmatrix} 1 & 0 \\ 0 & \frac{S_6}{S_5} \end{bmatrix} \begin{pmatrix} p_6 \\ \rho_o c_o u_6 \end{pmatrix} \qquad (10)$$

As described in Eq. (11), the four-pole matrix between points 7 and 8 (with mean flow) is

$$\begin{pmatrix} p_7 \\ \rho_o c_o u_7 \end{pmatrix} = \begin{bmatrix} 1 & 0 \\ 0 & \frac{S_8}{S_7} \end{bmatrix} \begin{pmatrix} p_8 \\ \rho_o c_o u_8 \end{pmatrix} \qquad (11)$$

2.4 Combination of system matrix

By using the matrix substitution in Eqs. (1)(2)(3)(4)(5)(7)(9)(10) and (11), one has

$$\begin{aligned}
&\begin{pmatrix} p_1 \\ \rho_o c_o u_1 \end{pmatrix} = e^{-jk\left(\frac{M_1 L_1}{1-M_1^2}+\frac{M_4 L_{3a}}{1-M_4^2}+\frac{M_6 L_{3b}}{1-M_6^2}+\frac{M_8 L_{3c}}{1-M_8^2}+\frac{M_{11} L_5}{1-M_{11}^2}\right)} \\
&\begin{bmatrix} \cos\left(\frac{kL_1}{1-M_1^2}\right) & j\sin\left(\frac{kL_1}{1-M_1^2}\right) \\ j\sin\left(\frac{kL_1}{1-M_1^2}\right) & \cos\left(\frac{kL_1}{1-M_1^2}\right) \end{bmatrix} \\
&\begin{bmatrix} Ts2_{1,1} & Ts2_{1,2} \\ Ts2_{2,1} & Ts2_{2,2} \end{bmatrix} \begin{bmatrix} \cos\left(\frac{kL_{3a}}{1-M_4^2}\right) & j\sin\left(\frac{kL_{3a}}{1-M_4^2}\right) \\ j\sin\left(\frac{kL_{3a}}{1-M_4^2}\right) & \cos\left(\frac{kL_{3a}}{1-M_4^2}\right) \end{bmatrix} \\
&\begin{bmatrix} 1 & 0 \\ 0 & \frac{S_6}{S_5} \end{bmatrix} \begin{bmatrix} \cos\left(\frac{kL_{3b}}{1-M_6^2}\right) & j\sin\left(\frac{kL_{3b}}{1-M_6^2}\right) \\ j\sin\left(\frac{kL_{3b}}{1-M_6^2}\right) & \cos\left(\frac{kL_{3b}}{1-M_6^2}\right) \end{bmatrix} \begin{bmatrix} 1 & 0 \\ 0 & \frac{S_8}{S_7} \end{bmatrix} \\
&\begin{bmatrix} \cos\left(\frac{kL_{3c}}{1-M_8^2}\right) & j\sin\left(\frac{kL_{3c}}{1-M_8^2}\right) \\ j\sin\left(\frac{kL_{3c}}{1-M_8^2}\right) & \cos\left(\frac{kL_{3c}}{1-M_8^2}\right) \end{bmatrix} \begin{bmatrix} Ts8_{1,1} & Ts8_{1,2} \\ Ts8_{2,1} & Ts8_{2,2} \end{bmatrix} \\
&\begin{bmatrix} \cos\left(\frac{kL_5}{1-M_{11}^2}\right) & j\sin\left(\frac{kL_5}{1-M_{11}^2}\right) \\ j\sin\left(\frac{kL_5}{1-M_{11}^2}\right) & \cos\left(\frac{kL_5}{1-M_{11}^2}\right) \end{bmatrix} \begin{pmatrix} p_{12} \\ \rho_o c_o u_{12} \end{pmatrix} \\
&= \begin{bmatrix} T_{1,1} & T_{1,2} \\ T_{2,1} & T_{2,2} \end{bmatrix} \begin{pmatrix} p_{12} \\ \rho_o c_o u_{12} \end{pmatrix}
\end{aligned} \qquad (12)$$

Therefore, the sound transmission loss (STL) of a muffler is defined as [4]

$$\begin{aligned}
&STL\begin{pmatrix} Q, f, L_1, L_2, L_{3a}, L_{3b} \\ , L_{3c}, L_4, D_1, D_2, D_3 \end{pmatrix} \\
&= 20\log\left(\frac{\left|T_{1,1}+T_{1,2}+T_{2,1}+T_{2,2}\right|}{2}\right) \\
&+ 10\log\left(\frac{S_1}{S_{12}}\right)
\end{aligned} \qquad (13)$$

III. CSAE STUDY

The shape optimization of noise elimination on a diesel engine is introduced as the case for simulation. The sound pressure level (SPL) at the exhausted outlet is investigated below:

f(Hz)	63	125	250	500	1k	2k	4k	8k
SPL	79	83	82	93	84	80	77	53

indicated in the data, the sound energy at 500 Hz is remarkable. An optimal design is tried on the muffler at the specific frequency (*f*) of 500 Hz. For maintenance and operation purposes in the machine room, the space of the silencer is then constrained at 0.5 meter in width, 0.5 meter in height and 3.0 meter in length. The O.D. of the exhaust pipe at both ends is confined to 0.0762 (m). In order to simplify the optimal process, an assumption of the symmetric geometry on the muffler (comprised of two identical chambers) is then made. This is translated into $L_2 = L_4$; $L_{3a} = L_{3c}$; $L_1 = L_5$. The space constraint for the muffler is shown in Fig.3. The design volume flow rate (Q) is confined to 0.8(m^3/s). The graphic

analysis and numerical assessments are developed as follows:

IV. COMPUTER AIDED DESIGN

4.1 Sensitivity analysis

4.1.1 D2 and f effect

The STL (with respect to D_2) and the frequency is shown in Fig.4. As indicated in Fig. 4, the gain of STL will be inversely increased when D_2 is decreased at the fixed frequency. Obviously, the gain effect in STL is dominated by D_2.

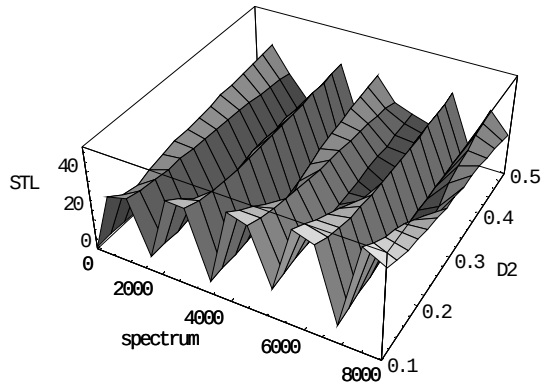

Fig.4. STL with respect to D_2 and frequency.

4.1.2 L_{3a} and D_{45} effect

The STL with respect to L_{3a} and D_{45} is shown as Fig.5. As shown in Fig.5, the variety of STL with respect to L_{3a} at 500Hz is in periodic form. Moreover, *STL* becomes larger when D_{45} is increased. Visibly, both L_{3a} and D_{45} have high sensitivity to STL. Consequently, L_{3a} is the key-parameter resulting in frequency shifting. Respectively, D_{45} is the powerful parameter in the gain of STL.

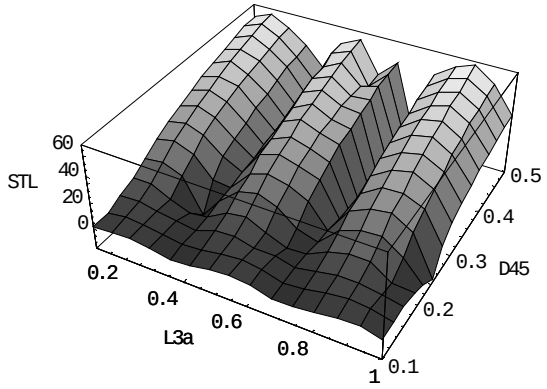

Fig.5. STL with respect to D_{45} and L_{3a}

4.1.3 L_{3b} and D_{45} effect

The response of STL with respect to L_{3b} and D_{45} at 500Hz is plotted in Fig.6.

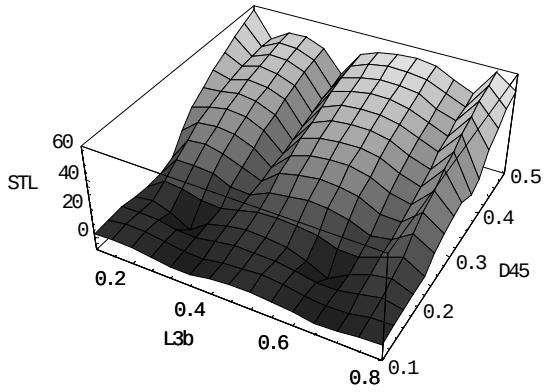

Fig.6. STL with respect to D_{45} and L_{3b}

As revealed in Fig.6, the periodic variety to L_{3b} and the proportionally increased curve to D_{45} are demonstrated.

Both L_{3b} and D_{45} are the effective design

parameters to STL. Conclusively, the parameter of L_{3b} is a determining factor in tuning the frequency. On the other hand, the parameter of D_{45} is highly related to the gain of STL.

4.1.4 L_{3a} and L_{3b} effect

The STL with respect to L_{3a} and L_{3b} is shown as Fig.7. Figure 7 reveals that both L_{3a} and L_{3b} are various with a periodic form with respect to STL (at 500Hz). The four peak values of STL with respect to L_{3a} and L_{3b} are discovered simultaneously. Both L_{3a} and L_{3b} are sensitive concurrently. They are the essential factors in tuning the wave frequency.

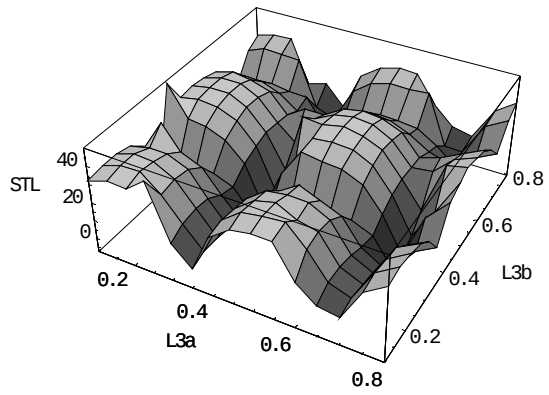

Fig.7. STL with respect to L_{3a} and L_{3b}

4.2 Discussion of sensitivity

Based on the analysis of Section 4.1, D_{45}, L_{3a}, L_{3b}, and D_2 are the effective parameters possessing higher sensitivity to STL. According to Fig.5 and 6, the STL is in direct proportion to D_{45}.

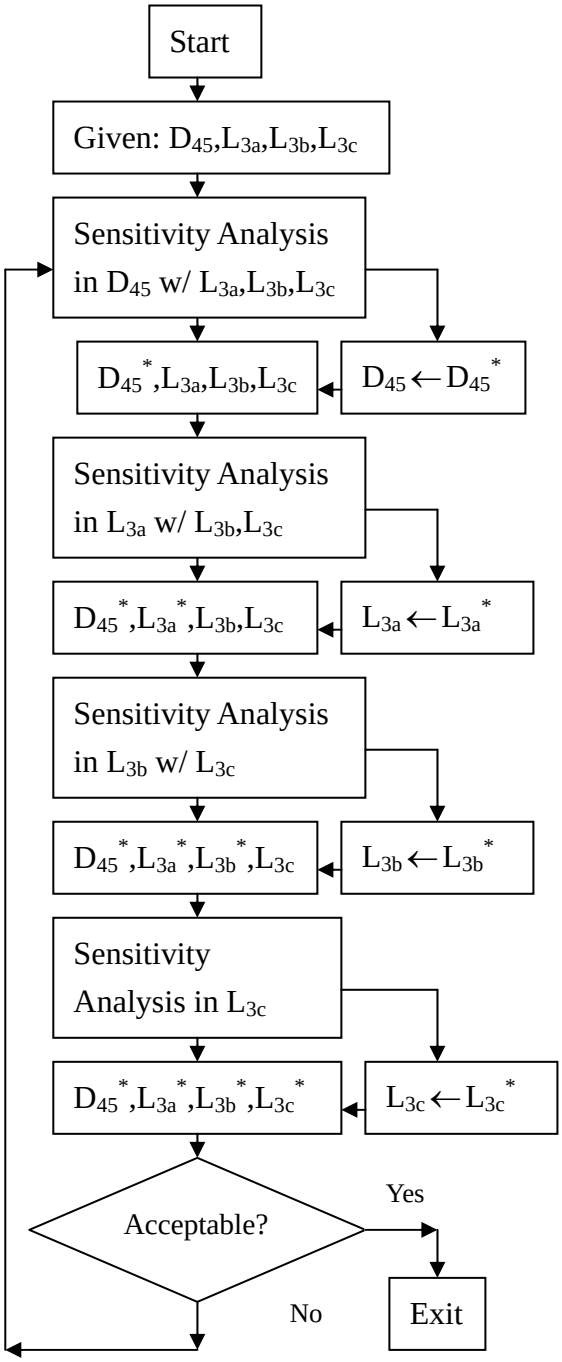

Fig.8. Algorithm of graphic searching technique.

In order to better manufacture the muffler, an assumption of L_1 and L_5 not less than 0.1(m) is introduced. The maximum value of D_{45} is

set at 0.3 (m). Consequently, the three parameters (L_{3a}, L_{3b} and D_2) are thus taken into consideration in the optimization. The algorithm flow chart used in the graphic searching technique (for the initial design data) is presented and shown in Fig. 8.

By using the algorithm of the graphic searching technique together with the graphic system (as seen in Fig. 4 and 7), the initial design data for each parameter is achieved and listed as follows.

D_{45}=0.1 (m); L_{3a}=0.2 (m); L_{3b}=0.6 (m)

V. NUMERICAL OPTIMAL ASSESSMENT

In order to maximize the value of STL, the minimal value of –STL(X) is planned and carried out. The three parameters (L_{3a}, L_{3b} and D_2) are chosen during the following numerical optimization processes:

5.1 Mathematical formulation [7, 8]

Minimize $F(X)$ = –STL(X) Objective function

Subject to: $g_j(X) \le 0 \quad j = 1,3$

inequality constraints

where $X = \begin{bmatrix} X_1 \\ X_2 \\ X_3 \end{bmatrix} = \begin{bmatrix} L_{3a} \\ L_{3b} \\ D_2 \end{bmatrix}$

design variable

$D_{45} \ge D_2 \ge 0.0762$; $L_{3a} \ge 0$; $L_{3b} \ge 0$;
$L_o = L_2 + L_{3a} + L_{3b} + L_{3c} + L_4$; $D_{45} = 0.3$

The initial design data is $(X_1, X_2, X_3)_{Starting\_pt} = (0.2, 0.6, 0.1)$. In order to obtain the numerical design data, two kinds of search algorithms are used in the optimal design process and are introduced as follows:

5.1.1 Exterior penalty function method [7, 8]

In the exterior penalty function method (EPFM), Φ is assembled by penalizing the objective function when constraints are violated $(g_i(X) > 0)$,

$$\Phi(X, r_p) = F(X) + r_p.P(X)$$

$$= F(X) + r_p \sum_{i=1}^{5} \{\max[0, g_i(X)]\}^2$$

where
$g_1(X) = -X_1$; $g_2(X) = -X_2$;
$g_3(X) = 0.5X_2 - 0.5L_o + X_1$;
$g_4(X) = 0.0762 - X_3$; $g_5(X) = X_3 - D_{45}$

The constraints are squared in order to ensure a continuous slope of the penalty and the pseudo-object functions (at the constraint boundary). For lower values of the penalty factor, the pseudo-object function is well behaved. The algorithm of the exterior penalty function method (EPFM) is shown in Fig. 9.

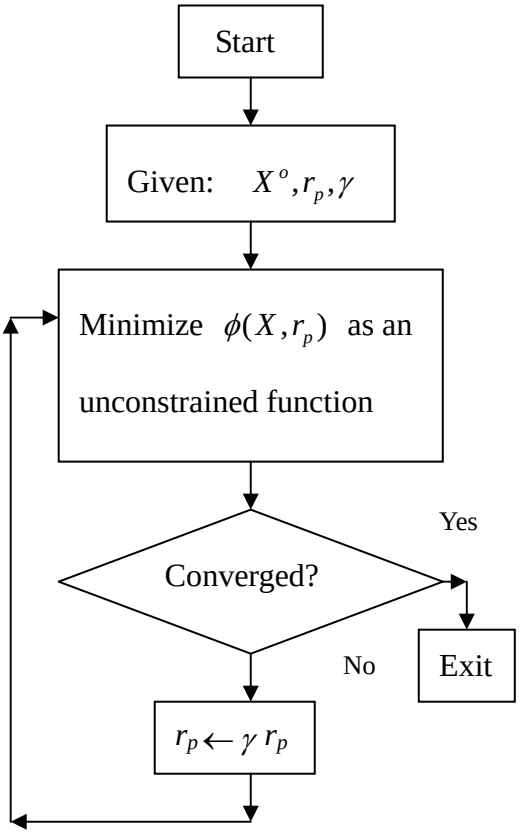

Fig.9. Algorithm of EPFM [7, 8].

5.1.2 Interior penalty function method [7, 8]

The interior penalty function method (IPFM) for inequality constraints is a sequence of improving designs whereby the constrained optimum is approached from inside the feasible region.

By using interior penalty function method, Φ is defined as

$$\Phi(X, r_p', r_p) = F(X) + r_p' \sum_{j=1}^{5} \frac{-1}{g_j(X)}$$

where

$g_1(X) = -X_1$; $g_2(X) = -X_2$;

$g_3(X) = 0.5X_2 - 0.5L_o + X_1$;

$g_4(X) = 0.0762 - X_3$; $g_5(X) = X_3 - D_{45}$

The choice of large penalty factors should be exercised so that steeper slopes (at the constraint boundaries) and smaller penalty terms are reached. The search procedure must also start from within and should not leave the feasible ranges. This IPFM is frequently applied for imposing parameter side constraints (where one can simply choose the feasible starting values). The algorithm of the interior penalty function method is shown in Fig. 10.

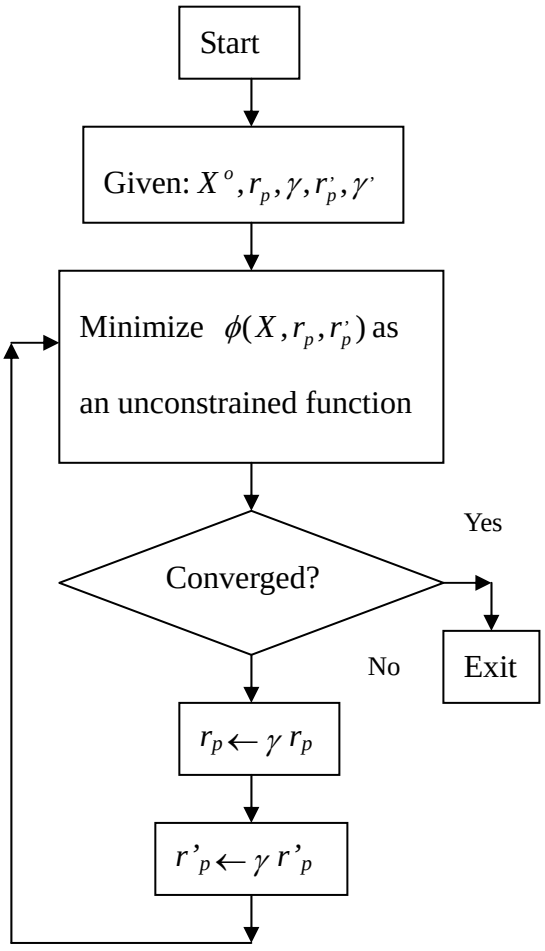

Fig.10. Algorithm of IPFM [7, 8].

5.2 Iteration and results

By assigning the initial design data as the first trial value, a successive iteration with the search algorithms (such as EPFM or IPFM) is then applied individually. The optimal STL with respect to the optimal design parameters (by the above two methods) are summarized and listed in Table 1.

Table 1. Optimal STL with respect to the optimal design parameters in two methods

Method	L_{3a}	L_{3b}	D_2	STL
EPFM	0.33501	0.614094	0.11402	241.1
IPFM	0.42772	0.428679	0.17880	204.8

$\{\overline{X}\}_1 = (0.427729, 0.428679, 0.178807)$
$\{\overline{X}\}_2 = (0.335017, 0.614094, 0.114023)$;

Table 1 reveals that the STL of EPFM is better than that of IPFM. Therefore, the 1st design data optimized by EPFM is adopted. The STL (of which at the 1st optimized design data) is plotted in Fig. 11. Figure 11 shows that the noise reduction effect of the muffler (241.1 dB at 500Hz) is acceptable.

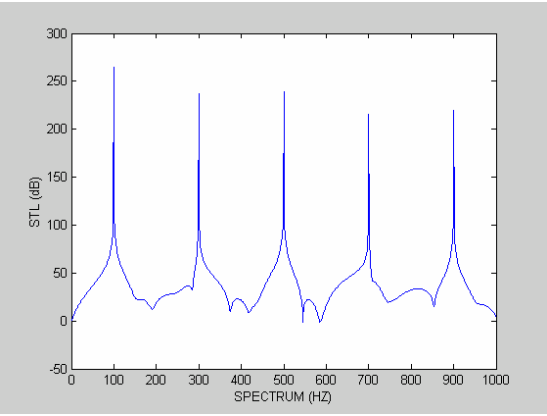

Fig.11. Optimal STL with respect to frequency.

5.3 Accuracy

In order to verify the accuracy of the study, Kuhn-Tucker's necessary conditions are then applied in order to check the convergence criterion in each optimality approach [7, 8]. The Kuhn-Tucker Condition is described as follows:

$$(1)\ \lambda_j g_j(X^*) = 0 \qquad j = 1,3 \qquad \lambda_j \geq 0 \ ;$$

$$(2)\ R(X^*) = \nabla F(X^*) + \sum_{j=1}^{3} \lambda_j \nabla g_j(X^*)$$

Table 2 Results of Kuhn-Tucker Condition's checking process in EPFM and IPFM

Method	Residual Vector		
	$\{R_1\}$	$\{R_2\}$	$\{R_3\}$
EPFM	-.39E-02	-.19E-02	0.0
IPFM	0.26E+05	.19E-02	0.0

In order to meet the converge criterion, the conditions of "$R(X^*) \approx 0$" and "$\lambda_j \geq 0$" are needed. By taking $\{\overline{X}\}_1$ and $\{\overline{X}\}_2$ into Kuhn-Tucker Condition's checking process, Table 2 reveals that the residual vectors in the 1st design data is closer to that in the 2nd design data. Again, the accuracy check demonstrates that the 1st solution is better

than the other.

VI. CONCLUSIONS

The space reserved for maintenance inside a confined machine proves essential in the equipment layout. There is an increasing interest in designing mufflers within a limited space.

In this paper, the theoretical STL of double-chamber mufflers (hybridized with side inlet/ outlet tube is deduced) and the computer's graphic system presents a quick examination of all the global peak points and the decisions of sensitivity analysis for each design parameter. Using the proposed scheme for graphic analysis on sensitivity, one set of design data is primarily determined from the chart. Using the fundamental data as initial design value, two kinds of searching techniques were introduced for the optimization process of the muffler. The Kuhn-Tucker Condition is also applied to verify the accuracy of the solution. This study not only arranges the best design of double-chamber mufflers but also provides an effective optimization approach to the constraint problem occurring in the practical engineering field.

REFERENCES

[1] Tracor Inc., Guidelines on Noise, American Petroleum Institute, Washington D.C., p. 55, 1973.

[2] Prasad, M. G., "A Note on Acoustic Plane Waves in a Uniform Pipe with Mean Flow," Journal of Sound and Vibration, Vol. 95, No. 2, pp. 284-290, 1984.

[3] Munjal, M. L., "Plane Wave Analysis of Side Inlet/Outlet Chamber Mufflers with Mean Flow," Applied Acoustics, Vol. 52, pp. 165-175, 1997.

[4] Munjal, M. L., Acoustics of Ducts and Mufflers with Application to Exhaust and Ventilation System Design, John Wiley & Sons, New York, 1987.

[5] Bernhard, Robert J., "Shape Optimization of Reactive Mufflers," Noise Control Engineering Journal, Vol. 27, No. 1, pp. 10-17, 1986.

[6] Yeh, L. J., Chiu, M. C., and Lai, G. J., " Computer Aided Design on Single Expansion Muffler under Space Constraints," Proceedings of the 19th National Conference on Mechanical Engineering, The Chinese Society of Mechanical Engineers, Hu-wei, Taiwan, C7, pp. 625-633, 2002.

[7] Vanderplaats, Garret N., Numerical Optimization Techniques for Engineering Design: with Applications, McGraw-Hill, New York, 1984.

[8] Weeber, K., Ratnajeevan S.and Hoole H., "Geometric Parametrization and Constrained Optimization Techniques in the Design of Salient Pole Synchronous Machines," IEEE Transaction on Magnetics, Vol. 28, No. 4, pp. 1948-1960, 1992.

[9]

NOMENCLATURE

C_o sound speed (m s^{-1})

D_o total width of muffler (m)

D_1 diameter of side inlet duct (m)

D_2 diameter of inter-connecting duct (m)

D_3 diameter of side outlet duct (m)

j $\sqrt{-1}$

k wave number

k_c, k_e stagnation pressure loss factor

L_o total length of muffler (m)

L_1 length of side inlet duct (m)

L_2 length of first chamber from edge to pt.3 (m)

L_{3a} length of first chamber from pt. 4 to pt. 5 (m)

L_{3b} length of inter-connecting duct (m)

L_{3c} length of second chamber from pt. 9 to pt. 8 (m)

L_4 length of second chamber from edge to pt. 10 (m)

L_{45} width of chambers (m)

L_5 length of side outlet duct (m)

M_i mean flow Mach number at pt. i

p_i pressure; acoustic pressure at pt. i (Pa)

Q venting volume flow rate at exhaust pipe (m^3/s)

S_i section area of duct at pt. i (m^2)

STL sound transmission loss (dB)

SPL sound pressure level (dB)

u_i acoustic particle velocity at pt. i (m s^{-1})

v_i acoustic mass velocity at pt. i (kg s^{-1})

Y_i characteristic impedance at pt. i

Z_i impedance at pt. i

ρ_o air density (kg m^{-3})